The Mechanism of Formation of Amide-Based Interlocked Compounds: Prediction of a New Rotaxane-Forming Motif

David A. Leigh,*[a] Alessandro Venturini,*[b] Andrew J. Wilson,[a] Jenny K. Y. Wong,[a] and Francesco Zerbetto*[c]

Abstract: Molecular modeling of four different reagent systems shows that the (free) energies of supramolecular interactions in the gas phase and in solution can explain the different reaction products (i.e., various sized macrocycles, catenanes, and linear oligomers) that are formed in classic amide-catenane-forming reactions. Self-assembly of the catenanes requires the formation of ordered intertwined chains and is driven by bifurcated hydrogen bonds, with π stacking only playing a lesser role. The understanding gained from the computational study was used to predict the possibility of a new rotaxane-forming system that does not permit catenane formation. The predictions were confirmed by the successful synthesis and characterization (including X-ray crystallography) of two novel rotaxanes.

Keywords: catenanes · molecular modeling · reaction mechanisms · rotaxanes · self-assembly

Introduction

In 1992 Hunter reported[1] the chance discovery of the first of what would prove to be a remarkably structurally diverse family of amide-based interlocked molecular species. Amide-based catenanes,[2–23] for example, cat(**1**),[11] are formed during the multicomponent condensations of aromatic (usually 1,3-) diacid chlorides and hindered bianilines or benzylic diamines in nonpolar solvents (Scheme 1). Also formed in the reactions are the corresponding un-interlocked macrocycles (of various sizes), linear oligomers, and, at least in some cases,[21,24–26] topologically nontrivial knots.

[a] Prof. D. A. Leigh, A. J. Wilson, J. K. Y. Wong
School of Chemistry, University of Edinburgh
The King's Buildings, West Mains Road
Edinburgh, EH9 3JJ (UK)
Fax: (+44) 131-667-9085
E-mail: david.leigh@ed.ac.uk

[b] Dr. A. Venturini
ISOF, Consiglio Nazionale delle Ricerche
via Gobetti 101, 40129 Bologna (Italy)
Fax: (+39) 051-639-8349
E-mail: a.venturini@isof.cnr.it.

[c] Prof. F. Zerbetto
Dipartmento di Chimica "G. Ciamician"
Università degli Studi di Bologna
via F. Selmi 2, 40126 Bologna (Italy)
Fax: (+39) 051-209-9456
E-mail: gatto@ciam.unibo.it

Supporting information for this article is available on the WWW under http://www.chemeurj.org/ or from the author.

Several features of the reactions are particularly worthy of note:

1) Catenanes are only formed in relatively nonpolar solvents (e.g., $CHCl_3$, CH_2Cl_2, chlorobenzene). The use of more polar solvents (e.g., acetone, DMF) gives rise only to macrocycles and linear oligomers.
2) Although the reaction is remarkably structurally tolerant, some acid chlorides (e.g. 2,4,5,6-tetrafluorobenzene 1,3-diacid chloride[12]) do not form catenanes, yielding only macrocycles and linear oligomers. The amount of catenane and macrocycle formed, and also their ratio, varies depending on the structures of the particular acid chlorides and amines used.
3) Except in special cases,[21] the only macrocycles formed in appreciable quantities during the reactions are those resulting from 2+2 (major) and 4+4 (minor) condensations of the bis-acid chloride and bis-amine. The 3+3 macrocycle is only formed in trace amounts.
4) In the presence of suitable stoppered threads (e.g., 1,3-diamides,[27] peptides,[28–31] fumaramides,[32–34] bis-nitrones,[35] etc.) the catenane-forming reactions also yield rotaxanes. In such cases, considerably more of the 2+2 macrocycle is produced in total (in the combined forms of "free" 2+2 macrocycle, rotaxane, and catenane) in these reactions than is formed in the absence of the thread.[27]
5) Other acyl leaving groups (activated esters, anhydrides, isocyanates, etc.) also work in the reaction, but acid chlorides give the highest yields of catenanes.

  DOI: 10.1002/chem.200305662

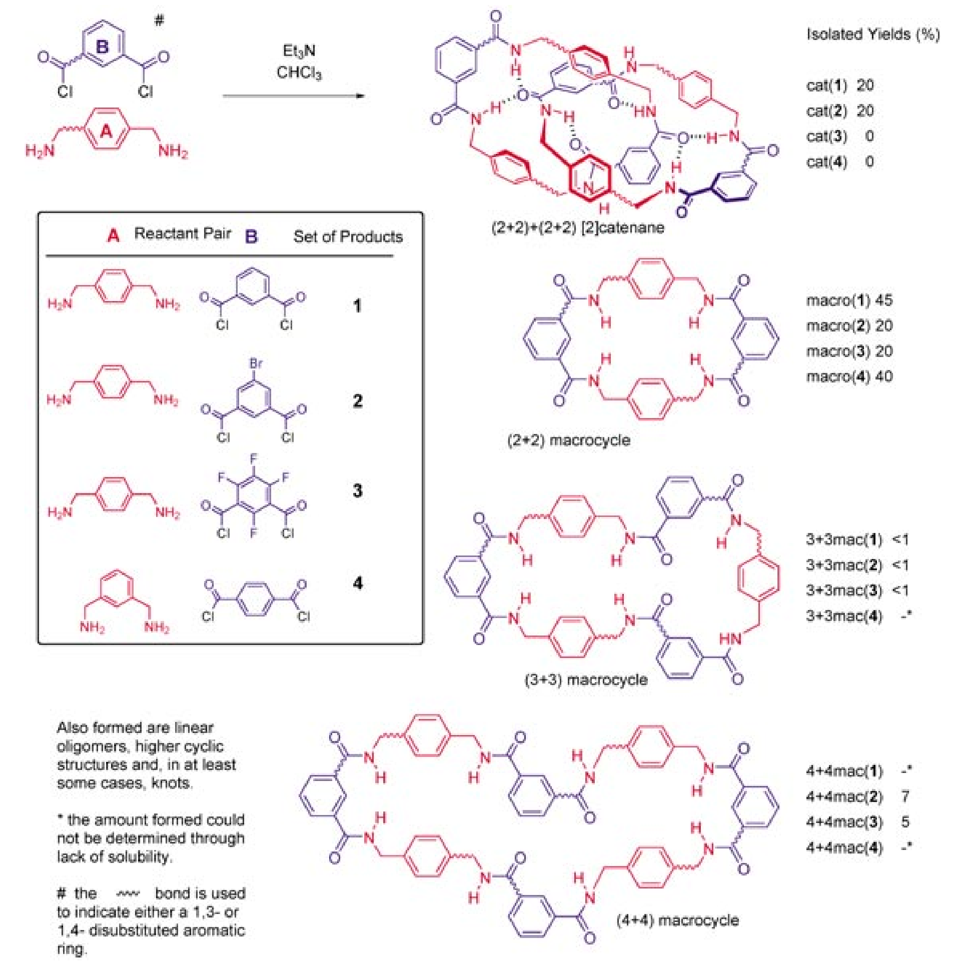

Scheme 1.

6) Bifurcated hydrogen bonds and quadruple π stacks of aromatic rings are seen extensively throughout the crystal structures of the mechanically-interlocked products.[4,11,13,28–32,36–40]

Despite the many examples that have been reported over the past decade, mechanistic explanations of the reaction have proved unsatisfactory. Particular stereochemical outcomes have been "explained" by invoking what are at best unlikely chemical arguments, including the preferential orientation of a simple guest in a virtually symmetrical macrocycle binding site,[3] or the binding of functional groups,[5] for example, acid chlorides, which are known to be poor hydrogen bond acceptors[41] (and have since been shown not to bind strongly to these types of amide-based macrocycles as an isolated functional group type[28,42]). Here we describe a computational study that provides a clear basis for the general reaction mechanism and explains the observations listed above. The proposed mechanism can be used to rationalize experimentally observed departures from the "standard" product distribution and to predict new strategies for hydrogen-bond-directed synthesis. In particular, a new hydrogen-bond motif for rotaxane formation—indeed, one that does not permit catenane formation!—is predicted and successfully demonstrated.

Nomenclature: In its simplest form, the amide-based catenane-forming reaction involves an aromatic 1,3-diacid chloride, for example, isophthaloyl dichloride, and a diamine, for example, xylylene diamine. To simplify the discussion, the following notation is used: The two basic units are labelled A for diamino fragments and B for the diacyl units. Open oligomers are indicated by a string of letters such as ABAB. Terminal A and B residues possess amine and acid chloride end groups, respectively. Adjacent A and B units are connected by an amide bond. A hyphen is used to denote a supramolecular adduct of two species, for example, ABAB-AB. The 2+2 macrocycles are abbreviated to macro, 3+3 macrocycles to 3+3mac, 4+4 macrocycles to 4+4mac, and the catenanes to cat. The intermediates and products arising from a particular reaction pairing are indicated by parenthesized suffices **1** to **4**. For example, ABAB-AB(**1**) is the supramolecular complex of the open chain tetramer and the AB fragment of **1**; analogously ABAB-AB indicates the same system for all four species. The nomenclature system used is bifrontal (unlike peptide or nucleic acid sequences), that is, BABA = ABAB.

Method: A combination of reversible (the formation of individual weakly bonding interactions, π stacks, and hydrogen bonds, various conformational and co-conformational changes) and irreversible (covalent amide bond formation) steps controls 1) the build up of linear fragments (A + B → AB; AB + AB → ABAB; AB + B → BAB etc), 2) the first ring closure to form the 2+2 macrocycle (ABAB → macro) and, where possible, the subsequent interlocking to form the catenane (ABAB-macro → cat).

Four different pairs of reactants were selected for study because they lead to different product distributions (Scheme 1): reactant pair **1**: 1,4-xylylenediamine, benzene-1,3-diacid chloride; reactant pair **2**: 1,4-xylylenediamine, 5-bromobenzene-1,3-diacid chloride; reactant pair **3**: 1,4-xylylenediamine, 2,4,5,6-tetrafluorobenzene-1,3-diacid chloride; reactant pair **4**: 1,3-xylylenediamine; benzene-1,4-diacid chloride.

The product distributions for three (**1**–**3**) of the reagent pair systems have previously been reported.[11,12] The fourth reagent system (**4**), reversing the regiochemistry of the amines and acid chlorides on the aromatic rings, yields macrocycle but no catenane and has not previously been described.

The observation[27] that in the presence of a suitable thread, considerably more macrocycle is produced than in the simple catenane-forming reaction, suggests that the first macrocyclization (ABAB→macro) benefits from the activity of a template (i.e., ABAB-X→macro-X). X could potentially be a reactant, such as the initial diamine (A) or acid chloride (B), a reaction by-product such as chloride ion, a reaction intermediate made up of an open chain sequence of A and B units, or a combination of these things. Since the second cyclization step, interlocking, proceeds in much higher yields than could be accounted for by nonassisted statistical threading,[43,44] it clearly proceeds via a supramolecular macro-ABAB precursor. Both the ABAB-X type and the macro-ABAB adducts owe their stability to supramolecular interactions, which must provide a driving force able to overcome processes that compete with the two ring closures. These include the uncoiling of reaction intermediate chains, the unthreading of the ABAB fragment from the macrocycle, and the formation of longer chains (oligomer and polymer formation).

Computational background: We examined all of the 29 sets of bimolecular adducts that could feature during the course of each reaction and the seven sets of molecular fragments that make up the supramolecular adducts. Together these span all the possible variations (open chains and rings) that might arise along the catenane-forming pathway from the individual reactants to the macrocycle–tetramer supramolecular complex, which is the immediate precursor of catenane formation. Two adducts containing pentamers were also considered to assess the potential for the polymerization of the reactions.

The co-conformation of each pair and the conformation of its components was "simulated annealed" to locate the most stable structure within the MM3* molecular mechanics procedure implemented in the Macromodel program.[45] MM3* is similar to the MM3 procedure[46] that has found wide application[35,40,47] to treat the properties of this class of molecules. The two force fields differ in some technical details:

1) The electrostatic equation—MM3* uses partial charges and Coulomb's law, while MM3 uses bond dipoles and Jean's equation.
2) The out-of-plane bending equation—MM3* uses an improper torsion, while MM3 uses a pyramidalization distance.
3) The π-electron conjugation—MM3* parameterizes the bond orders, while MM3 calculates them by a self consistent field, SCF, procedure. Bypassing the SCF procedure results in a considerable reduction in computer time and is, in fact, the only practical way of carrying out the required simulated annealing study.
4) The way amides are parameterized was modified. Default parameterization was used so that in the amide group, the C=O and NH fragments were considered separately. We have previously found that this approach is important in order to accurately reproduce experimental data for the structure and dynamics of benzylic amide macrocycle-containing catenanes and rotaxanes.

All the calculations were performed both with and without an implicit solvent model,[48–50] which was used to simulate the presence of $CHCl_3$. Both the energy and the free energy, ΔG_{298}, were calculated [Eq. (1)]:

$$\Delta G_{298} = E(MM+) - RT \ln Q \tag{1}$$

In Equation (1) Q is the nuclear motion, that is, the vibrational, partition function. Occasionally, the vibrational contribution modified the order of stability of the most stable isomers. Whenever possible the lowest ΔG values were used. Importantly, adduct formation introduces some very low frequency vibrations that are supra- or intermolecular vibrations. While the net effect must be calculated, it may be expected that the potential energy profiles will be affected upon going from ΔE to ΔG_{298}.

Results and Discussion

The experimental yields of macrocycle and catenane formation in reactant systems **1**–**3** have previously been reported.[11,12] The isophthaloyl chloride, *p*-xylylenediamine system **1** produces both the 2+2 macrocycle and catenane in ~45% and 20% yields, respectively. A slightly lower yield of the 2+2 macrocycle is observed with the 5-bromoisophthaloyl chloride system (**2**). The perfluorinated isophthaloyl unit (**3**) results in no catenane formation, but the 2+2 macrocycle is still formed. The fourth reactant system (1,3-xylylenediamine; benzene 1,4-diacid chloride; **4**) yields no catenane and 40% of the 2+2 macrocycle.

Clearly, variations in the strength of the supramolecular binding motifs (normal versus bifurcated hydrogen bonding, pairing versus multiple π stacking, van der Waals, dipole–dipole interactions, etc.) selects ring closure over either the further growth of a linear chain or precipitation from solution. However, the calculations cannot be compared directly with reaction yields, since the (free) energy of formation of the amide bonds is not included in a directly comparable way by the force field model.[51] However, one can quantitatively compare the interaction energies of all the different species calculated as the difference between the energies of each adduct and the energy of its components at infinite separation. We have therefore used the calculations in this way to understand qualitative differences—for example, significant amounts of catenane or no catenane formed, whether 2+2 macrocycle or higher oligomerization is favored, whether 3+3 or 4+4 macrocycle formation is preferred, and so forth—in the behavior of the different reactant pairs.

Importantly, it must be kept in mind that the self-assembly is driven by the irreversible formation of the C–N bond. The investigation of the relative stabilities of the 29 pairs provides information on the product distribution only under the reasonable assumption that the energy of the transition state for C–N bond formation of a more stable pair is lower than that of a less stable pair. Such energy is the sum of the intrinsic activation energy for C–N formation, which should be similar in all the steps of the self-assembly, plus the non-bonding interactions that occur in the activated complex, which we assume are similar to those of the product. When the interaction energy of the two components of the pair is large the product is lower in energy and the preceding transition state is concomitantly lower in energy. As usual in reactivity, the picture is that of a steep downhill slope (to the products) after a hill (the transition state). Here, however, the deeper is the energy minimum, the lower the previous hill was to surmount, because similar stabilizing interactions are present in the transition state and in the product.

The energy profiles allow catenane formation only for 1 and 2: The first issue to address is whether the calculations reproduce the different distribution of the reaction products of the four sets of reagent pairs. Figure 1 shows the free energies at 298 K (ΔG_{298}) in chloroform; the results shown are those directly related to the experimental data and they will be discussed here in detail, while the data of the energies and free energies in gas phase are shown and discussed briefly in the Supporting Information.

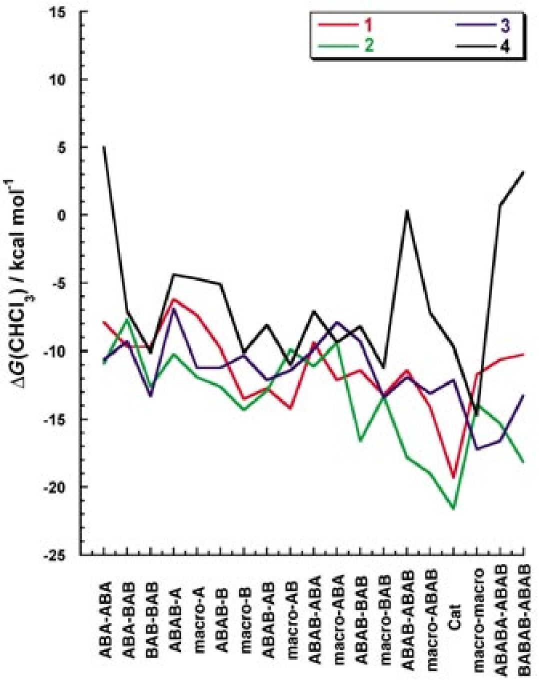

Figure 1. Free energies at 298 K (ΔG_{298}) in chloroform. The lines between the points are only provided to assist the eye and do not imply the actual pathway of the reaction.

The energy profile of **1** and **2** converge to the minima of the corresponding catenanes. For **3**, the global minimum is the macro–macro dimer(**3**) (-17.2 kcal mol^{-1}) indicating the greater difficulty of forming catenanes using reactant systems **3**, that is, it provides an explanation for why it is not observed. A similar situation occurs in the energy profile of **4**, although some of the intermediates are now highly unstable. The cat(**4**) (-9.7 kcal mol^{-1}) is 5.0 kcal mol^{-1} less stable than the macrocycle dimer(**4**) (-14.7 kcal mol^{-1}), showing no driving force for catenane formation. Extension of a chain to form a pentamer produces an increase in energy with respect to the catenane for **1** with BABAB-ABAB(**1**) (-10.1 kcal mol^{-1}) less stable than ABABA-ABAB(**1**) (-10.6 kcal mol^{-1}), whereas for system **2**, BABAB-ABAB(**2**) (-18.2 kcal mol^{-1}) is more stable than ABABA-ABAB(**2**) (-15.3 kcal mol^{-1}). In **3**, the un-interlocked dimer remains the minimum and is not superseded by ABABA-ABAB(**3**) (-16.6 kcal mol^{-1}). The un-interlocked dimer of **4** remains the global minimum, since BABAB-ABAB(**4**) (3.2 kcal mol^{-1}) and ABABA-ABAB(**4**) (0.7 kcal mol^{-1}) are much above it. Comparison of the seven amide systems energies of the four species finds only the open-chain pairs of **3** lower in energy than the corresponding macro-ABAB adduct and, therefore, suggests that polymerization can occur for **3** via ABABA-ABAB(**3**).

The (free) energy profile of Figure 1, agrees with the experimental findings that **1** and **2** form both the 2+2 macrocycle and the catenane, while for **3** and **4** only the 2+2 macrocycle is observed. Reagent system **3** may be thermodynamically predisposed to oligomerize beyond the key ABAB tetrameric precursor to 2+2 macrocycle (and catenane). A key outcome of the calculations is that the self-templating ability of reagent system **4** is consistently lower than in systems **1** and **2**. If **4** were to be provided with a better template, it seems possible that interlocking could occur.

Some geometrical considerations: While it is not possible to extract details of the reaction pathway from the calculations, inspection of the structures in chloroform provides additional information about the ring closures. Specifically: 1) at which point the self-assembly routes followed by **1** and **2** diverge from those followed by **3** and **4**, 2) the conformation of the acyclic ABAB precursor to 2+2 macrocycle formation, 3) the template-catalyzed ring closure to form the 2+2 macrocycle, 4) why the 4+4 macrocycle is often produced in the reactions but not the 3+3 analogue, and 5) the driving force for [2]catenane formation.

Figure 2 shows the shortest distances between the reacting C and N terminals of the ABAB-X systems. From the profiles of the four species, it can be seen that the ABAB chain ends of ABAB-X are similar for **1** and **2**. The largest differences in distances (2.3 Å) are found for X = BAB and for the two complexes with the pentamers. Initially, **3** has a trend similar to that of **1** and **2**, but divergence occurs when X is a trimer (it is already very marked for X = ABA). Species **4** follows a different profile for the incipient C–N bond distance of ABAB from **1**, **2**, and **3**. Importantly, however, the C–N distance of macro-ABAB is similar for the four species. Formation or lack of formation of the catenane is apparently, therefore, not due to the spatial arrangement of the ABAB tetramer threaded through the macrocycle, since in all cases the chain ends would be sufficiently close together to react.

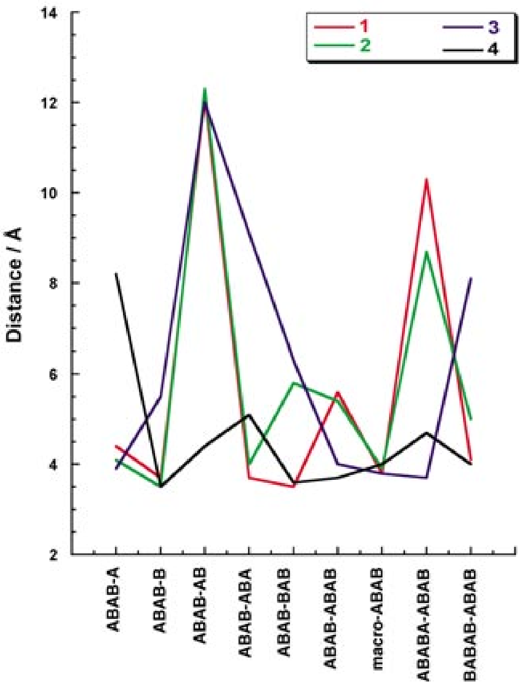

Figure 2. Distances in chloroform for the reacting carbon and nitrogen atoms in ABAB-X systems.

2+2 Macrocycle formation: In order to ascertain how the ABAB systems benefit from the templating effect of another chain to form the 2+2 macrocycle, we examined the most stable structures of ABAB(**1**)–(**4**) in solution (Figure 3). Despite the rather different profiles in Figures 1 and 2, all the ABAB fragments possess rather similar minimum energy structures, all with a *syn–anti* relationship for the amides of the internal B residue. This makes the ABAB fragment essentially linear, holding the reactive end groups far apart, making it long lived in solution. In the presence of a suitable template X, however, the most stable co-conformations have a *syn–syn* structure for the internal isophthalamide residue. This introduces a pronounced bend into the molecule, bringing the reactive end groups close together so that rapid cyclization occurs.

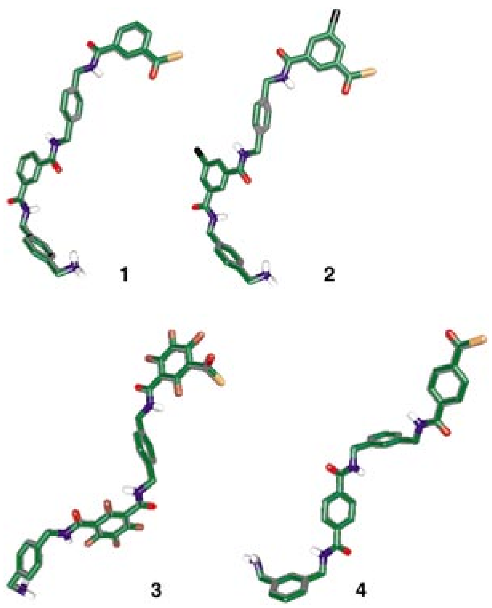

Figure 3. Most stable structures of ABAB in chloroform.

ABAB-X systems in which the incipient C–N bond length is large require a substantial torsional and spatial rearrangement of the two molecules to bring the chain ends closer. Implicitly, this makes the relation between stability of product pair and transition state energy no longer valid. On the assumption that the associated energy penalty excludes them as candidates for the ring closure to the 2+2 macrocycle, one can 1) set a C–N distance threshold (for instance, 4.2 Å) for the closure to the 2+2 macrocycle and 2) further select the ABAB-X systems on the basis of the energy difference with respect to the corresponding macro-X product.

For **1**, the types of X that promote a short incipient C–N distance are B, BAB, and ABA. The free energy differences between macro-X and ABAB-X are −1.8, +0.2, −0.7 kcal mol^{-1}, respectively. The moieties B and ABA (and to a lesser extent BAB) are therefore likely to catalyze 2+2 macrocycle formation.

For **2**, X = A (+2.5 kcal mol^{-1}), B (+2.5 kcal mol^{-1}), and ABA (+5.9 kcal mol^{-1}) give a short incipient C–N distance (in brackets, the free energy difference between macro-X and ABAB-X). Notice that macro(**2**) is formed together with the catenane through the energy gained by the amide CN condensation.

For **3**, X = A (+4.3 kcal mol^{-1}) and ABAB (−1.2 kcal mol^{-1}) gives a short incipient C–N distance. The ABAB-ABAB arrangement is therefore likely to cyclize one ring, but it is not followed by a second closure to form a catenane.

For **4**, X = B (+0.5 kcal mol^{-1}), BAB (+2.5 kcal mol^{-1}), and ABAB (−1.9 kcal mol^{-1}) produce a short incipient C–N distance. The ABAB fragment is therefore likely to catalyze the first ring formation, but not the second.

Larger macrocycles—3+3 versus 4+4: Table 1 shows the shortest distances between the reactive C and N terminals found by the calculations in various adducts required to form 3+3 and 4+4 macrocycles. The separation of the reacting C and N terminals for ABA-BAB and ABAB-AB are, on average, larger than those of ABAB-ABAB. Although longer distances may be compatible with ring closure, as seen with the 2+2 ring formation, large distances are often associated with substantial energy barriers that could prevent ring closure. Setting the same 4.2 Å threshold **1**, **2**, and **3** should only close to form the 4+4 macrocycle. Neither the 3+3mac nor 4+4mac of **4** should be produced in large amounts, a finding in agreement with experiment.

Table 1. Calculated distances, Å, between the reacting C and N terminals required to form 3+3 and 4+4 macrocycles in $CHCl_3$.

	1		**2**		**3**		**4**	
	3+3	4+4	3+3	4+4	3+3	4+4	3+3	4+4
	5.1	8.8	5.6	8.4	6.7	13.7	7.4	8.4
ABA-BAB	6.3	12.6	5	11.7	8.5	8.7	6.6	18.2
ABAB-AB	5	6.4	5.1	6.3	5.6	6.9	6.1	6.9
ABAB-ABAB	4.2	5.5	4.2	5.3	3.3	3.9	7.5	10.1

The driving force for[2]-catenane formation: The structures of the ABAB-X adducts can help us understand the growing number of interactions formed during the [2]catenane assembly process. Figure 4–7 give a pictorial representation of the growing sequence for the four species, which are ABAB-AB, ABAB-ABA, ABAB-BAB, ABAB-ABAB, and ABAB-macro. A more detailed presentation is given in Table 2, in which five principal noncovalent binding motifs are identified. Three of them are connected with π stacking, namely a four-layered stack, a three-layered sandwich, and the π complex; the remaining two are regular two center hydrogen bonds and bifurcated hydrogen bonds.

For both **1** and **2**, the π motif evolves from a simple stack to a final four-layered stack or quadruple-decker. The initial two regular hydrogen bonds tend to be replaced by bifurcated ones along the sequence, so that in the largest structures there is only one standard hydrogen bond, while there are two or three bifurcated hydrogen bonds.

For **3**, the π motif also evolves from a simple stack to a four-layered stack. The number of hydrogen bonds is largest (i.e., three) for ABAB-ABAB (which the results described earlier suggested as the likely intermediate for macrocycle formation), while only macro-ABAB shows two bifurcated hydrogen bonds.

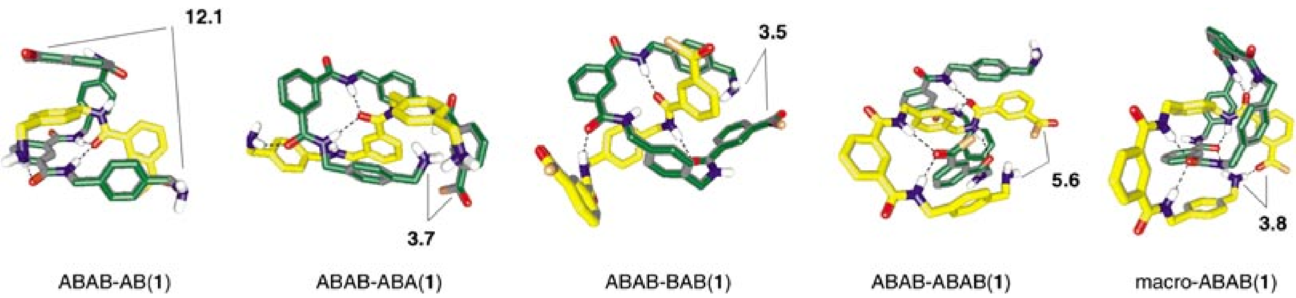

Figure 4. ABAB-X supramolecular adducts for **1**.

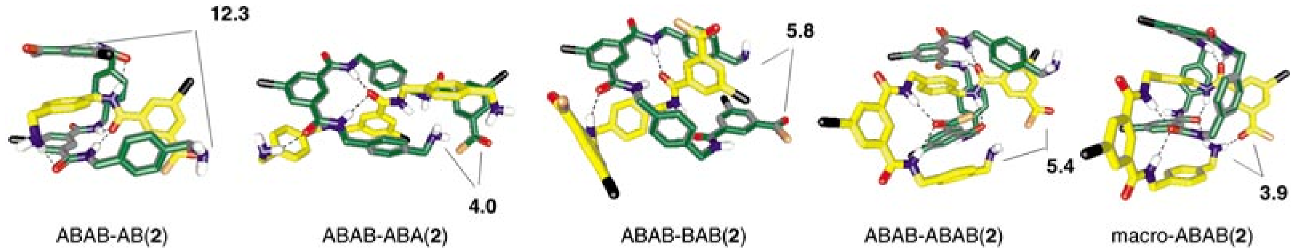

Figure 5. ABAB-X supramolecular adducts for **2**.

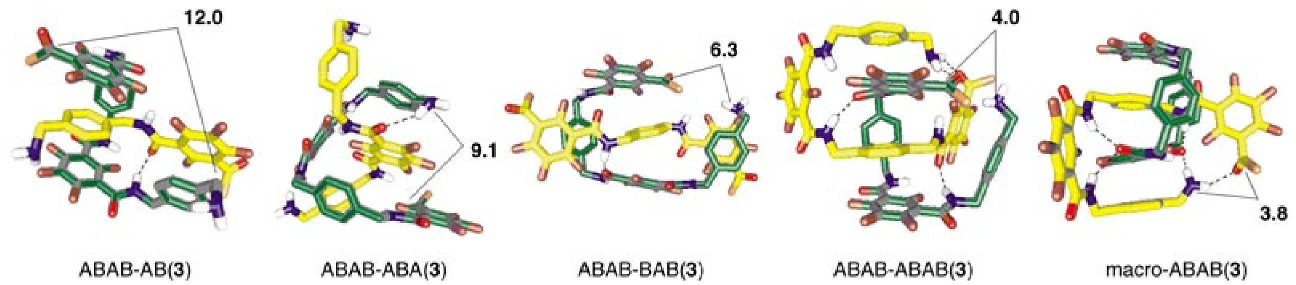

Figure 6. ABAB-X supramolecular adducts for **3**.

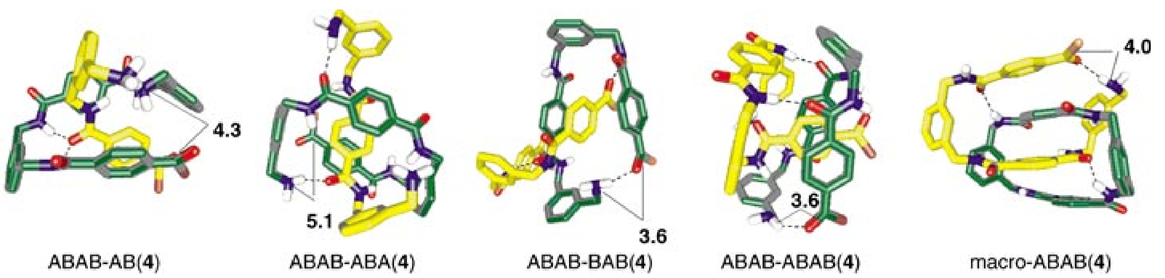

Figure 7. ABAB-X supramolecular adducts for **4**.

Table 2. Number of various noncovalent bonding motifs in the ABAB-X adducts in systems **1**–**4**.

	Quadruple π stack				Triple π stack				Single π stack				Two center hydrogen bond				Bifurcated hydrogen bond			
	1	**2**	**3**	**4**	**1**	**2**	**3**	**4**	**1**	**2**	**3**	**4**	**1**	**2**	**3**	**4**	**1**	**2**	**3**	**4**
ABAB-AB	0	0	0	0	1	1	1	0	1	1	1	1	2	2	1	0	1	1	0	1
ABAB-BAB	1	1	0	0	0	0	1	1	0	0	2	0	2	2	1	3	1	1	0	0
ABAB-ABA	0	0	0	0	1	1	1	1	0	0	0	0	1	1	2	2	1	1	0	0
ABAB-ABAB	1	1	1	0	0	0	0	1	1	1	0	0	1	1	3	3	2	2	0	0
macro-ABAB	1	1	1	1	0	0	0	0	0	0	0	0	1	1	2	3	3	3	2	0

For **4**, the π motif ultimately becomes a quadruple-decker stack. The number of hydrogen bonds soon reaches a maximum of three, while few bifurcated hydrogen bonds are present.

It can be concluded that while all the species share similar π-stacking structures, the major difference between **1** and **2** on one side, and **3** and **4** on the other, is the presence of bifurcated hydrogen bonds in the self-assembled adducts as they increase in size. The possibility of forming bifurcated hydrogen bonding—found ubiquitously in both their X-ray crystal structures and those of the related family of rotaxanes—therefore appears to be the hallmark for catenane formation.

More on π stacking—when is it effective?: All the reaction systems **1** to **4** build up, ultimately, to a quadruple π-stacking motif in the final products. The question arises if π stacking influences the pathway of the self-assembly or if it is an additional motif brought about by the presence of hydrogen bonds and flexible chains.

The energetics of the π stacks of benzene rings and tetrafluorinated benzene rings (as in **3**) can shed light on this issue. It is known that benzene forms a dimer π stack with a stabilization energy of 2–3 $kcal\,mol^{-1}$. The present model was actually parameterized to reproduce it and gives 2.4 $kcal\,mol^{-1}$. Fluorine substitution, as in **3**, in one of the two benzenes increases the stabilization energy to -6.3 $kcal\,mol^{-1}$. Analogously, the energy of interaction of a benzene quadruple-decker is -7.4 $kcal\,mol^{-1}$ and substitution of every other benzene with a fluorinated molecule further lowers it to -19.0 $kcal\,mol^{-1}$. In $CHCl_3$, all the values are strongly affected and increased, that is, made less negative. The benzene dimer is now unstable by 0.5 $kcal\,mol^{-1}$; the dimer with one fluorinated and one normal benzene is stable by only -2.3 $kcal\,mol^{-1}$. A benzene quadruple stack goes up to 1.4 $kcal\,mol^{-1}$. Notice that the system is still in a minimum, but is thermally unstable. The mixed stack of two normal and two fluorinated benzene rings is instead binding at -7.0 $kcal\,mol^{-1}$. While the addition of substituents to the benzene rings, such as the amide groups, probably deepens the minima, it is concluded that during the self-assembly in chloroform, π stacks are not the driving force and the hydrogen-bond pattern largely determines the products formed.

Testing the mechanism—prediction of a new rotaxane-forming motif: The reason that reagent system **4** does not form [2]catenanes appears to be its low tendency to self-complex, which is reflected in the "higher" position the relevant profiles have in Figures 1 and 2. Indeed, the 2+2 macrocycle formed with reagent system **4** would be isomeric (and have the same ring size in terms of atoms) with the 2+2 macrocycle formed with **1**. The key hydrogen-bond donor groups can even adopt similar positions to those in 2+2mac(**1**), but transposing the amide carbonyl groups with the benzylic methylene groups alters the shape of the ring (changes conjugation patterns, the regions in which it is flexible or rigid, etc.) to such an extent that it does not "thread" correctly. In practice, the absence of an internal isophthalamide group destabilizes the pair structures and the transition state that leads to the adduct is concomitantly higher. The calculations show that upon folding in the complex the hydrogen-bond-donating groups of ABAB(**4**) and ABAB(**1**) are in similar places, so the ABAB(**4**) fragment should cyclize in roughly the same way as the analogous isophthalamide and 5-bromoisophthalamide systems. Since it is impossible to make cat(**4**), we decided to use this system to check if directed hydrogen bonding was strong enough to overcome this problem in the presence of a suitable template. The idea was to try assembling a macrocycle about peptide and fumaramide threads that are extremely effective templates for cyclization of the ABAB(**1**) fragment, as evidenced by the high yields of the corresponding rotaxanes. Since ABAB(**4**) seems to retain many of the structural features of ABAB(**1**)—perhaps surprisingly given the changes that varying the regiochemistry of the amides might be expected to bring—it seemed possible that the directed hydrogen bonding in these systems might be strong enough to act as good templates and overcome the self-complexing deficiency of **4**.

This hypothesis turned out to be correct. Treatment of appropriate glycylglycine (glygly) and fumaramide threads with reagent system **4** led to the formation of glygly rot(**4**) and fumaramide rot(**4**) in 20 and 30% yields, respectively (Scheme 2). Crystals suitable for investigation by X-ray crystallography were obtained for both rotaxanes from the slow evaporation of solutions in ethanol (glygly rot(**4**)) or a chloroform/methanol mixture (fumaramide rot(**4**)). A comparison of these crystal structures with those of the known reagent pair **1** analogues, glygly rot(**1**) and fumaramide rot(**1**), is shown in Figure 8. It reveals that the A (bisamine) and B (bisacyl) units simply switch places in **1** and **4** for both types of thread. This necessarily distorts the geometry of the macrocycle in **4** (Figure 8a and b compared to c and d), in particular breaking the conjugation of the amide groups with the aromatic ring in the terephthalamide macro-

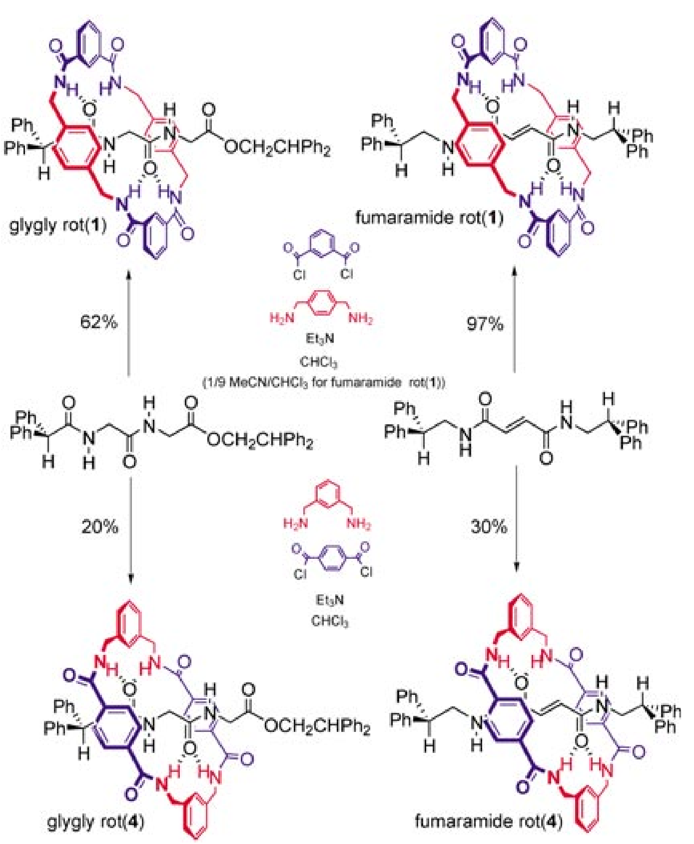

Scheme 2.

cycle. It is fascinating that the peptide and fumaramide templates are sufficiently strong binding sites to do this in the ABAB-X precursor to rotaxane formation so that it competes with the rapid ABAB→macro cyclization process. The corresponding ABAB-macro complex, of course, does not. It would require twice as many high energy distortions of the terephthalamide units in the catenane precusor to do this, not only two in the ABAB fragment but also two in the macro part as well. The peptide and fumaramide threads, of course, do not require any high energy distortions to make an effective template.

Conclusions

The synthesis of benzylic amide-based macrocycles and catenanes is a highly versatile and structurally tolerant process. However, what might appear to be slight variations in the reactants can actually result in major changes in the formation of specific ring sizes and the occurrence or absence of interlocked structures. The calculated (free) energy profiles, and in particular the free energies of supramolecular interactions in chloroform, can rationalize these experimental findings. Reagent systems **1** and **2** both form catenanes, as well as 2+2 and, probably, 4+4 macrocycles. The supramolecular energy of interaction suffices to introduce enough weakly bonding interactions to give ring closures to both macrocycle and catenane. The simple reason why **3** does not form the catenane is that the un-interlocked dimer of the macrocycle is more stable than the interlocked system; and the reaction has a clear tendency to oligomerize beyond the necessary tetrameric species. In **4** the same experimental lack of catenane formation is caused by poor self-templating ability. In all cases the calculations show that formation, or lack of formation, of the catenane is not due to the spatial arrangement of the precursor, that is, macro–ABAB, which are all characterized by similar distances between the atoms of the incipient amide C−N bond, but to the relative (free) energy of the macro-ABAB pseudo rotaxane. The calculations also show that π stacking is not the major force for the self-assembly and that the difference between **1** and **2** on the one side, and **3** and **4** on the other, is the presence of bifurcated hydrogen bonds in the self-assembled pairs as they grow in size. The possibility of

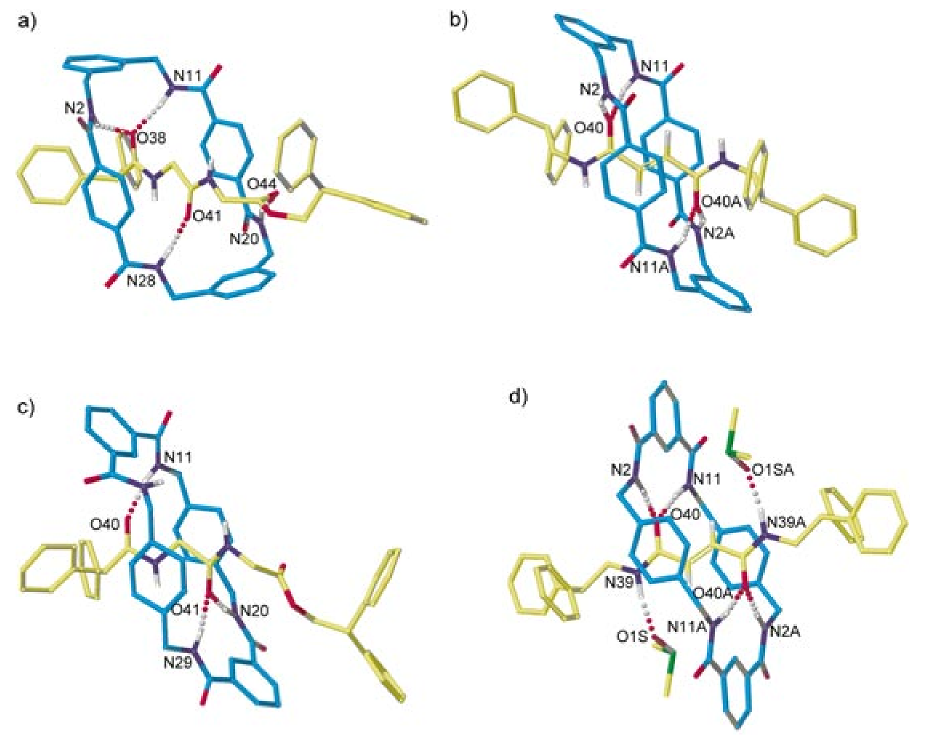

Figure 8. X-ray crystal structures of a) glygly rot(**4**), b) fumaramide rot(**4**), c) glygly rot(**1**) and d) fumaramide rot(**1**). For clarity carbon atoms of the macrocycle are shown in blue and the carbon atoms of the thread in yellow; oxygen atoms are depicted in red, nitrogen atoms dark blue, and selected hydrogen atoms white. Intramolecular hydrogen bond lengths [Å] and angles [°]: a) O38−N2 3.29, 152.0; O38−N11 2.91, 158.7; O41−N28 2.82, 150.7; O44−N20 3.03, 162.6; b) O40−N2/O40A−N2A 2.98, 151.4; O40−N11/O40A−N11A 3.11, 145.9; c) O40−N11 2.87, 165.3; O41−N20 3.19, 170.1; O41−N29 3.01, 174.0; d) O40−N2/O40A−N2A 3.20, 173.7; O40−N11/O40A−N11A 2.95, 169.3; N39−O1S/N39A−O1SA 2.85, 169.7.

forming bifurcated hydrogen bonding is the hallmark for amide catenane formation.

Finally, the insight gained from such a computational study can be used to make predictions about product distributions and to design new reaction strategies for the noncovalent-directed synthesis of interlocked architectures. The understanding of the non-catenane-forming pathway for **4** was used to predict and then demonstrate that rotaxanes could still be produced from a suitable amide-ring-forming reagent system that does not form catenanes, the first time that this has been demonstrated in supramolecular-directed synthesis.

Experimental Section

Glygly rot(4): Solutions of *meta*-xylylene diamine (1.08 g, 7.91 mmol) in anhydrous chloroform (50 mL) and terephthaloyl dichloride (1.61 g, 7.91 mmol) in anhydrous chloroform (50 mL) were added, simultaneously over a period of four hours by means of motor-driven syringe pumps, to a stirred solution of the glycylglycine thread (0.50 g, 0.99 mmol) and triethylamine (2.2 mL, 15.80 mmol) in anhydrous chloroform (150 mL). When addition was completed the reaction mixture was allowed to stir for a further eighteen hours, after which time the reaction mixture was filtered and the filtrate was washed with hydrochloric acid (0.2 M, 100 mL) and saturated sodium bicarbonate solution (100 mL). The organic layer was then dried over magnesium sulphate and filtered, and the solvent removed under reduced pressure. The rotaxane glygly rot(**4**) was isolated by column chromatography (silica gel, 10% EtOAc/CH_2Cl_2). Yield: 0.28 g (20%); m.p. 154.5–156.3 °C; ^{1}H NMR (400 MHz, $CDCl_3$): δ = 2.04 (d, J = 4.5 Hz, 2H; NHCH_2CO), 2.49 (d, J = 5.0 Hz, 2H; NHCH_2CO), 3.19 (t, J = 8.0 Hz, 1H; CHCH$_2$), 4.41 (dd, J = 14.0, 5.0 Hz, 6H; CH_2NHCO$_{\text{macrocyclic}}$ and CHCH_2 from COSY), 4.47 (s, 1H; CHCO), 4.58 (dd, J = 14.0, 5.5 Hz, 4H; CH_2NHCO$_{\text{macrocyclic}}$), 5.44 (t, J = 4.5 Hz, 1H; NH), 6.04 (t, J = 5.0 Hz, 1H; NH), 6.98 (t, J = 5.0 Hz, 4H; NH), 7.15–7.22 (m, 16H; ArCH), 7.23–7.37 ppm (m, 20H; ArCH); ^{13}C NMR (100 MHz, [D$_6$]DMSO): δ = 40.52 (CH_2), 41.69 (CH_2), 43. 77 (CH_2), 49.29 (CH), 56.31 (CH), 67.13 (CH_2), 127.07 (ArCH), 127.26 (ArCH), 128.04 (ArCH), 128.13 (ArCH), 128.27 (ArCH), 128.53 (ArCH), 128.74 (ArCH), 128.81 (ArCH), 128.92 (ArCH), 128.94 (ArCH), 137.49 (q, ArC), 139.07 (q, ArC), 140.28 (q, ArC) 141.64 (q, ArC), 166.22 (CO) 167.00 (CO), 168.15 (CO) 173.03 ppm (CO); FAB-MS (*m*BNA matrix): *m/z*: 1039 [M+H]$^+$; elemental analysis calcd (%) for $C_{64}H_{58}N_6O_8$ (1038): C 73.97, H 5.63, N 8.09; found: C 73.78, H 5.83, N 7.99.

Fumaramide rot(4): Solutions of *meta*-xylylene diamine (1.08 g, 7.91 mmol) in anhydrous chloroform (50 mL) and terephthaloyl dichloride (2.61 g, 7.91 mmol) in anhydrous chloroform (50 mL) were added, simultaneously over a period of four hours by means of syringe pumps, to a stirred solution of the fumaramide thread (0.50 g, 0.99 mmol) and triethylamine (1.60 g, 2.20 mL, 15.80 mmol) in anhydrous chloroform (150 mL). When addition had been completed, the reaction mixture was allowed to stir for a further eighteen hours, after which time the reaction mixture was filtered and the filtrate washed with hydrochloric acid (0.2 M, 100 mL) and saturated sodium bicarbonate solution (100 mL). The organic layer was then dried over magnesium sulfate and the solvent removed under reduced pressure. The rotaxane fumaramide rot(**4**) was isolated by column chromatography (silica gel, 2% methanol/CH_2Cl_2); Yield: 0.32 g, 30%; m.p. 329.9–331.9 °C; ^{1}H NMR (400 MHz, [D$_6$]DMSO): δ = 3.77 (t, J = 6.5 Hz, 4H; CHCH_2) 4.21 (t, J = 6.5 Hz, 2H; CHCH$_2$), 4.58 (d, J = 5.5 Hz, 8H; CH_2NHCO), 4.85 (s, 2H; COCHCHCO), 6.80 (s, 8H; ArCH$_F$), 7.19 (t, J = 7.5 Hz, 4H; ArCH), 7.31 (m, 22H; ArCH), 7.74 (s, 2H; ArCH$_C$), 8.00 (t, J = 5.5 Hz, 4H; CH$_2$NHCO$_{\text{macrocycle}}$), 8.35 ppm (t, J = 6.5 Hz, 2H; NHCOCH); ^{13}C NMR (100 MHz, [D$_6$]DMSO): δ = 43.37 (CH_2), 43.97 (CH_2), 50.76 (CH), 125.40 (ArCH), 126.54 (ArCH), 126.66, (ArCH), 126.93 (ArCH), 128.80 (ArCH), 128.91 (ArCH), 131.96 (ArCH), 132.08 (COCHCHCO), 138.15 (q, ArC), 139.54 (q, ArC), 143.21 (q, ArC), 165.30 (CO), 167.60 ppm (CO); FAB-MS (*m*BNA matrix): *m/z*: 1007 [M+H]$^+$; elemental analysis calcd (%) for $C_{64}H_{58}O_6N_6$ (1006): C 76.32, H 5.80, N 8.34; found C 75.96, H 5.83, N 8.19.

X-ray crystallographic structure determinations:

glygly rot(**4**): $C_{68}H_{66}N_6O_{10}$, M_r = 1127.27, crystal size 0.42 × 0.32 × 0.02 mm, monoclinic $P2_1/c$, colorless, a = 18.0678(3), b = 19.0166(4), c = 17.19790(10) Å, β = 99.8100(10)°, V = 5822.6(2) Å^3, Z = 4, ρ_{calcd} = 1.286 Mg m^{-3}; Mo$_{K\alpha}$ radiation (graphite monochromator, λ = 0.71073 Å), μ = 0.087 mm^{-1}, T = 180(2 K. 23 932 data (10 156 unique, R_{int} = 0.0906, $1.57 < \theta < 25.00°$), were collected on a Siemens SMART CCD diffractometer using narrow frames (0.3° in ω), and were corrected semi-empirically for absorption (transmission 0.79–0.96). The structure was solved by direct methods and refined by full-matrix least-squares on F^2 values of all data (G.M.Sheldrick, SHELXTL manual, Siemens Analytical *X*-ray Instruments, Madison WI, USA, 1994, version 5) to give $wR = \{\Sigma[w(F_o^2-F_c^2)^2]/\Sigma[w(F_o^2)^2]\}^{1/2} = 0.1902$, conventional R = 0.0819 for F values of 4803 reflections with $F_o^2 > 2\sigma F_o^2$), S = 1.046 for 771 parameters. Residual electron density extremes were 0.379 and −0.327 e Å^{-3}. Amide hydrogen atoms were refined isotropically with the remainder constrained; anisotropic displacement parameters were used for all non-hydrogen atoms.

Experimental details for fumaramide rot(**4**) were the same as for glygly rot(**4**) except for the following: $C_{66}H_{66}N_6O_8$, M_r = 1071.25, crystal size 0.50 × 0.40 × 0.40 mm, monoclinic $P2_1/n$, colorless, a = 9.9757(2), b = 18.3235(2), c = 16.7744(3) Å, β = 106.04 °, V = 2946.86(9) Å^3, Z = 2, ρ_{calcd} = 1.207 Mg m^{-3}; Mo$_{K\alpha}$ radiation (graphite monochromator, λ = 0.71073 Å), μ = 0.080 mm^{-1}, T = 180(2 K. 18 241 data (7113 unique, R_{int} = 0.0313, $2.22 < \theta < 29.01°$), were collected on a Siemens SMART CCD diffractometer using narrow frames (0.3° in ω), and were corrected semi-empirically for absorption (transmission 0.80–0.96). The structure was solved by direct methods and refined by full-matrix least-squares on F^2 values of all data (G.M.Sheldrick, SHELXTL manual, Siemens Analytical *X*-ray Instruments, Madison WI, USA, 1994, version 5) to give $wR = \{\Sigma[w(F_o^2-F_c^2)^2]/\Sigma[w(F_o^2)^2]\}^{1/2} = 0.1089$, conventional R = 0.0428 for F values of 4497 reflections with $F_o^2 > 2\sigma F_o^2$), S = 0.942 for 366 parameters. Residual electron density extremes were 0.198 and −0.211 e Å^{-3}.

CCDC-190622 (glygly rot(**4**)) and CCDC-190621 (fumaramide rot(**4**)) contain the supplementary crystallographic data for this paper. These data can be obtained free of charge via www.ccdc.cam.ac.uk/conts/retrieving.html (or from the Cambridge Crystallographic Data Centre, 12 Union Road, Cambridge CB21EZ, UK; fax: (+44) 1223-336-033; or deposit@ccdc.cam.uk).

Acknowledgement

This work was supported by European Union contracts IST-2001–35504 (MechMol) and HPRN-CT-2000–00024 (MIPA), the EPSRC, and MURST project "Dispositivi Supramolecolari". D.A.L. is an EPSRC Advanced Research Fellow (AF/982324).

[1] C. A. Hunter, *J. Am. Chem. Soc.* **1992**, *114*, 5303–5311.
[2] F. Vögtle, S. Meier, R. Hoss, *Angew. Chem.* **1992**, *104*, 1628–1631; *Angew. Chem. Int. Ed. Engl.* **1992**, *31*, 1619–1622.
[3] S. Ottens-Hildebrandt, S. Meier, W. Schmidt, F. Vögtle, *Angew. Chem.* **1994**, *106*, 1818–1821; *Angew. Chem. Int. Ed. Engl.* **1994**, *33*, 1767–1770.
[4] S. Ottens-Hildebrandt, M. Nieger, K. Rissanen, J. Rouvinen, S. Meier, G. Harder, F. Vögtle, *J. Chem. Soc. Chem. Commun.* **1995**, 777–778.
[5] F. Vögtle, R. Jäger, M. Handel, S. Ottens-Hildebrandt, *Pure Appl. Chem.* **1996**, *68*, 225–232.
[6] S. Baumann, R. Jäger, F. Ahuis, B. Kray, F. Vögtle, *Liebigs Ann./Recl.* **1997**, 761–766.
[7] F. Vögtle, O. Safarowsky, C. Heim, A. Affeld, O. Braun, A. Mohry, *Pure Appl. Chem.* **1999**, *71*, 247–251.
[8] A. Andrievsky, F. Ahuis, J. L. Sessler, F. Vögtle, D. Gudat, M. Moini, *J. Am. Chem. Soc.* **1998**, *120*, 9712–9713.

[9] O. Safarowsky, E. Vogel, F. Vögtle, *Eur. J. Org. Chem.* **2000**, 499–505.

[10] F. Schwanke, O. Safarowsky, C. Heim, G. Silva, F. Vögtle, *Helv. Chim. Acta* **2000**, *83*, 3279–3290.

[11] A. G. Johnston, D. A. Leigh, R. J. Pritchard, M. D. Deegan, *Angew. Chem.* **1995**, *107*, 1324–1327; *Angew. Chem. Int. Ed. Engl.* **1995**, *34*, 1209–1212.

[12] A. G. Johnston, D. A. Leigh, L. Nezhat, J. P. Smart, M. D. Deegan, *Angew. Chem.* **1995**, *107*, 1327–1331; *Angew. Chem. Int. Ed. Engl.* **1995**, *34*, 1212–1216.

[13] D. A. Leigh, K. Moody, J. P. Smart, K. J. Watson, A. M. Z. Slawin, *Angew. Chem.* **1996**, *108*, 326–331; *Angew. Chem. Int. Ed. Engl.* **1996**, *35*, 306–310.

[14] D. A. Leigh, A. Murphy, J. P. Smart, M. S. Deleuze, F. Zerbetto, *J. Am. Chem. Soc.* **1998**, *120*, 6458–6467.

[15] M. S. Deleuze, D. A. Leigh, F. Zerbetto, *J. Am. Chem. Soc.* **1999**, *121*, 2364–2379.

[16] T. J. Kidd, D. A. Leigh, A. J. Wilson, *J. Am. Chem. Soc.* **1999**, *121*, 1599–1600.

[17] N. Watanabe, Y. Furusho, N. Kihara, T. Takata, K. Kinbara, K. Saigo, *Chem. Lett.* **1999**, 915–916.

[18] Y. Furusho, J. Shoji, N. Watanabe, N. Kihara, T. Adachi, T. Takata, *Bull. Chem. Soc. Jpn.* **2001**, *74*, 139–147.

[19] N. Watanabe, N. Kihara, T. Takata, *Org. Lett.* **2001**, *3*, 3519–3522.

[20] N. Watanabe, Y. Furusho, N. Kihara, T. Takata, K. Kinbara, K. Saigo, *Bull. Chem. Soc. Jpn.* **2001**, *74*, 149–155.

[21] F. J. Carver, C. A. Hunter, R. J. Shannon, *J. Chem. Soc. Chem. Commun.* **1994**, 1277–1280.

[22] C. A. Fustin, C. Bailly, G. J. Clarkson, P. De Groote, T. H. Galow, D. A. Leigh, D. Robertson, A. M. Z. Slawin, J. K. Y. Wong, *J. Am. Chem. Soc.* **2003**, *125*, 2200–2207.

[23] D. A. Leigh, J. K. Y. Wong, F. Dehez, F. Zerbetto, *Nature* **2003**, *424*, 174–179.

[24] O. Safarowsky, M. Nieger, R. Fröhlich, F. Vögtle, *Angew. Chem.* **2000**, *112*, 1699–1701; *Angew. Chem. Int. Ed.* **2000**, *39*, 1616–1618.

[25] J. Recker, F. Vögtle, *J. Inclusion Phenom. Macrocyclic Chem.* **2001**, *41*, 3–5.

[26] F. Vögtle, A. Hünten, E. Vogel, S. Buschbeck, O. Safarowsky, J. Recker, A. H. Parham, M. Knott, W. M. Müller, U. Müller, Y. Okamoto, T. Kubota, W. Lindner, E. Francotte, S. Grimme, *Angew. Chem.* **2001**, *113*, 2534–2537; *Angew. Chem. Int. Ed.* **2001**, *40*, 2468–2471.

[27] A. G. Johnston, D. A. Leigh, A. Murphy, J. P. Smart, M. D. Deegan, *J. Am. Chem. Soc.* **1996**, *118*, 10662–10663.

[28] D. A. Leigh, A. Murphy, J. P. Smart, A. M. Z. Slawin, *Angew. Chem.* **1997**, *109*, 752–756; *Angew. Chem. Int. Ed. Engl.* **1997**, *36*, 728–732.

[29] W. Clegg, C. Gimenez-Saiz, D. A. Leigh, A. Murphy, A. M. Z. Slawin, S. J. Teat, *J. Am. Chem. Soc.* **1999**, *121*, 4124–4129.

[30] G. Brancato, F. Coutrot, D. A. Leigh, A. Murphy, J. K. Y. Wong, F. Zerbetto, *Proc. Natl. Acad. Sci. USA* **2002**, *99*, 4967–4971.

[31] T. Da Ros, D. M. Guldi, A. Farran Morales, D. A. Leigh, M. Prato, R. Turco, *Org. Lett.* **2003**, *5*, 689–691.

[32] F. G. Gatti, D. A. Leigh, S. A. Nepogodiev, A. M. Z. Slawin, S. J. Teat, J. K. Y. Wong, *J. Am. Chem. Soc.* **2001**, *123*, 5983–5989.

[33] F. G. Gatti, S. Leòn, J. K. Y. Wong, G. Bottari, A. Altieri, M. A. Farran Morales, S. J. Teat, C. Frochot, D. A. Leigh, A. M. Brouwer, F. Zerbetto, *Proc. Natl. Acad. Sci. USA* **2003**, *100*, 10–14.

[34] A. Altieri, G. Bottari, F. Dehez, D. A. Leigh, J. K. Y. Wong, F. Zerbetto, *Angew. Chem.* **2003**, *115*, 2398–2402; *Angew. Chem. Int. Ed.* **2003**, *42*, 2296–2300.

[35] V. Bermudez, N. Capron, T. Gase, F. G. Gatti, F. Kajzar, D. A. Leigh, F. Zerbetto, S. W. Zhang, *Nature* **2000**, *406*, 608–611.

[36] H. Adams, F. J. Carver, C. A. Hunter, *J. Chem. Soc. Chem. Commun.* **1995**, 809–810.

[37] A. Mohry, F. Vögtle, M. Nieger, H. Hupfer, *Chirality* **2000**, *12*, 76–83.

[38] Q. Y. Li, E. Vogel, A. H. Parham, M. Nieger, M. Bolte, R. Fröhlich, P. Saarenketo, K. Rissanen, F. Vögtle, *Eur. J. Org. Chem.* **2001**, 4041–4049.

[39] M. Asakawa, G. Brancato, M. Fanti, D. A. Leigh, T. Shimizu, A. M. Z. Slawin, J. K. Y. Wong, F. Zerbetto, S. W. Zhang, *J. Am. Chem. Soc.* **2002**, *124*, 2939–2950.

[40] F. Biscarini, M. Cavallini, D. A. Leigh, S. Leon, S. J. Teat, J. K. Y. Wong, F. Zerbetto, *J. Am. Chem. Soc.* **2002**, *124*, 225–233.

[41] M. H. Abraham, *Chem. Soc. Rev.* **1993**, *22*, 73–83.

[42] C. Seel, A. H. Parham, O. Safarowsky, G. M. Hubner, F. Vögtle, *J. Org. Chem.* **1999**, *64*, 7236–7242.

[43] E. Wasserman, *J. Am. Chem. Soc.* **1960**, *82*, 4433–4434.

[44] H. L. Frisch, E. Wasserman, *J. Am. Chem. Soc.* **1961**, *83*, 3789–3795.

[45] F. Mohamadi, N. G. J. Richards, W. C. Guida, R. Liskamp, M. Lipton, C. Caufield, G. Chang, T. Hendrickson, W. C. Still, *J. Comput. Chem.* **1990**, *11*, 440–467.

[46] N. L. Allinger, Y. H. Yuh, J. H. Lii, *J. Am. Chem. Soc.* **1989**, *111*, 8551–8582.

[47] M. Cavallini, R. Lazzaroni, R. Zamboni, F. Biscarini, D. Timpel, F. Zerbetto, G. J. Clarkson, D. A Leigh, *J. Phys. Chem. B* **2001**, *105*, 10826–10830.

[48] W. C. Still, A. Tempczyk, R. C. Hawley, T. F. Hendrickson, *J. Am. Chem. Soc.* **1990**, *112*, 6127–6129.

[49] W. Hasel, T. F. Hendrickson, W. C. Still, *Tetrahedron Comput. Methodol.* **1988**, *1*, 103.

[50] D. Qiu, P. S. Shenkin, F. P. Hollinger, W. C. Still, *J. Phys. Chem. A* **1997**, *101*, 3005–3014.

[51] Many other factors (e.g., solubility of the reagents, products and intermediates, reaction conditions, efficacy of purification methods) can also affect reaction yield.

Received: October 28, 2003
Revised: June 6, 2004
Published online: September 9, 2004

